Analysis of Computed Trajectories of Penetrant Micromolecules in a Simulated Polymeric Material

Constantine S. Chassapis,[†] John K. Petrou,[†] John H. Petropoulos,[*,†] and Doros N. Theodorou[†,‡]

Institute of Physical Chemistry and Molecular Modelling of Materials Laboratory, National Research Centre for the Physical Sciences "Demokritos", 15310 Ag. Paraskevi, Athens, Greece, and Department of Chemical Engineering, University of Patras, GR 26500 Patras, Greece

Received September 29, 1995; Revised Manuscript Received January 16, 1996[⊗]

ABSTRACT: Molecular dynamics trajectories of oxygen-like spherical molecules within a medium of eicosane-like chains at 303.5 K confined to a density very close to that of amorphous polyethylene are analyzed geometrically to elucidate mechanistic aspects of penetrant motion. To enable this analysis, reduced trajectories, *i.e.*, sets of equidistant positions along the paths of penetrant molecules, are constructed with various step lengths λ. The degree and prevailing direction of local orientation in the chain liquid are quantified through diagonalization of an orientation tensor defined in the vicinity of individual nodes or steps of the reduced trajectories. As in earlier simulation work, an anomalous (subdiffusive) regime is detected, which extends up to times of ∼150 ps or penetrant displacements of ∼1.5 nm. Directional correlations between steps of the reduced trajectory reveal that the penetrant is temporarily confined within elongated "cavities". The prevalent direction of chain orientation "seen" by the penetrant is found to persist over length scales of ∼2 nm. The degree of local anisotropy is lower along the penetrant trajectories than in the chain melt on average, because dense, strongly oriented regions can only form in the absence of penetrant. A weak but significant directional correlation is detected between penetrant displacements and the prevalent orientation of the surrounding polymer; the range of this correlation indicates that it is intimately related to anomalous diffusion. Over length scales of up to ∼1.5 nm, penetrant displacement is most facile along the backbones of chains. This is reminiscent of the idealized mechanistic model invoked in the Brandt and Pace and Datyner theories, although the degree of orientation is, of course, not nearly as large as suggested by that model.

1. Introduction

The rapidly developing practical applications of selective gas permeation through polymer membranes have stimulated intense interest in the underlying molecular diffusion mechanism. The classical theoretical approach to this problem is based on the Eyring transition-state theory: the diffusion process is viewed as a series of activated jumps.[1] In particular, it is considered that the penetrant molecule is normally confined by the surrounding polymer segments ("normal" or "resting" state) until the said segments happen, as a result of thermal fluctuations, to move in such a way as to open up sufficient space for a jump to occur ("activated" state).[2] The task of a fundamental theoretical model is, then, to evaluate the requisite activation energy, in terms of penetrant and polymer molecular parameters, by postulating typical "normal" and "activated" polymer segment configurations.

Most notable among such models is the one introduced by Brandt (B)[3] and developed further by Pace and Datyner (PD).[4] In the B-PD model, it is assumed that the polymer chains tend locally to lie parallel to each other. A penetrant is envisioned as spending most of its time in the interior of "bundles" of oriented chains (see Figure 1). It may jump out of a bundle through a process wherein segments of appropriate size on two neighboring chains in the bundle bend away from each other to form an opening through which the penetrant can pass. The crucial elementary diffusion jumps are thus pictured as occurring across the chains.[3] Pace and Datyner[4] have further elaborated this picture by pointing out that movement along the chains requires much less activation energy and should, therefore, be strongly preferred. But such movement is interrupted by entanglements; consequently, the observed diffusion process becomes rate-limited by the aforementioned energetically more costly jumps across the chains. Although this theoretical picture of micromolecular transport mechanism is of necessity highly idealized and oversimplified, it has, nevertheless, provided useful insights into the effects of various molecular polymer and penetrant parameters on gas permeability and permselectivity properties,[5] and it is still worthwhile, in our opinion, to refer to it for useful leads in connection with the analysis of the much more realistic (but correspondingly more complicated) picture that emerges from molecular computer simulation studies.

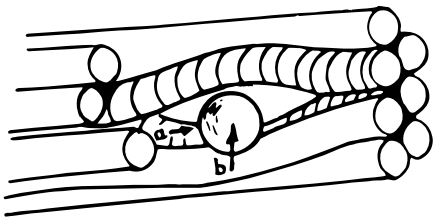

Figure 1. Molecular picture invoked in the model of Brandt and Pace and Datyner[3,4] illustrating the possibility of penetrant motion along (a) or across (b) the polymer chains (reproduced with permission from ref 4).

In the last few years, considerable molecular computer simulation work has been reported aiming either at direct prediction of diffusivities and solubilities of gaseous penetrants in amorphous rubbery and glassy

* Author to whom correspondence should be addressed. Phone: +30-1-6513112. FAX: +30-1-6522965. E-mail: petrop@cyclades.nrcps.ariadne-t.gr.
† NRCPS "Demokritos".
‡ University of Patras.
⊗ Abstract published in *Advance ACS Abstracts,* April 1, 1996.

S0024-9297(95)01474-4 CCC: $12.00

polymers or at the geometric or energetic analysis of regions accessible to gas molecules within polymer matrices and the elucidation of various mechanistic aspects of penetrant motion. Recently, this modeling work has been reviewed.[6,7]

Molecular dynamics simulation (MD) and transition-state theory-based analysis (TST) of the potential energy hypersurface of the polymer−penetrant system have emerged as two largely complementary approaches for the prediction of self-diffusivity. By its detailed nature, MD offers itself for mechanistic studies of gas molecule motion over time scales not exceeding tens of nanoseconds. Through such studies, the occurrence of jumplike penetrant migration has been established in polymers both above and below T_g. Relatively large gas molecules in dense polymers at low temperatures tend to spend most of their time confined within "cavities" and infrequently hop between neighboring cavities, taking advantage of thermal fluctuations in the polymer matrix that momentarily open short-lived passages or necks between the cavities. However, such hops are not always well-defined and become less so as temperature increases and/or penetrant size decreases.

Note that the term "cavity" as used here corresponds, in "geometric mapping" terms,[8,9] to a void in the polymeric matrix, all parts of which are freely accessible to a penetrant molecule with hard-sphere diameter equal to σ_A, in conjunction with a hard-sphere polymer segment diameter equal to σ_B (*cf.* "clusters of accessible volume" in ref 9). We shall use the term "cluster" or "string" of cavities to denote cavities linked by passages that will admit a molecule of hard-sphere diameter substantially less, but not much less, than σ_A (and still well above the maximum hard-sphere diameter of a molecule able to percolate right through the polymer matrix). In terms of potential energy mapping, a cavity will encompass adjacent energy minima (sorption sites) separated by very low (less than k_BT)[10] energy barriers (*cf.* "macrostates" in ref 11), while a penetrant molecule moving through a string of cavities will have to surmount barriers substantially higher than this, but still well below the observed activation energy of the overall transport process.

A remarkable recent finding is that diffusion in amorphous polymers exhibits a pronounced "anomalous" region at short times. Transport kinetics over this region has been described by a power law of the form $\langle \Delta r_A^2 \rangle \propto t^n$, with $n < 1$; in melts, crossover to the normal "Einstein" diffusive behavior $\langle \Delta r_A^2 \rangle \propto t$ have been observed to set in only at times of the order of 0.1−1 ns, the anomalous regime being more prolonged for more slowly diffusing systems.[6,10,12] Anomalous diffusion with $n < 1$ has also been detected in simulations of supercooled liquids governed by a Yukawa potential[13] and observed experimentally in quasi-two-dimensional systems of chains composed of magnetic dipolar particles in a magnetic field.[14] For solutes moving through liquids characterized by ordinary exclusion and London dispersion interactions, which are of interest in this study, anomalous diffusion is observed only when the liquid is polymeric and is evidently related to the long relaxation times that characterize polymer melts. According to Gusev *et al.*,[6] the structure of the slowly relaxing polymer matrix restricts the penetrant motion, so that, on the length scale of a few hopping distances, the penetrant's paths are not true random walks. The fact that the polymer environment gives rise to a separation of time scales consistent with the hopping mechanism (short-time in-cavity motion *versus* long-time diffusive motion) is seen as another cause of anomalous diffusion.[6] An alternative explanation[7,16] relates the anomalous regime to the broad distribution of rate constants that govern penetrant jumps.

Very recently, certain features of the van Hove self-correlation and intermediate scattering functions of MD micromolecular trajectories in a polyethylene-like medium, in the anomalous diffusion region, led Takeuchi and Okazaki[15] to the estimation of two characteristic spatial scales attributed to the microstructure of the polymer matrix and, in particular, to the mean size of cavities (referred to as "cages" in ref 15) and the mean distance between adjacent cavities (given as ∼0.3 and ∼0.6 nm, respectively). According to these authors, in-cage motion is primarily observed in the initial "ballistic" regime, whereas the anomalous diffusion encompasses the first few hops between cavities, in apparent agreement with the general ideas of Gusev *et al.*[6] quoted above.

We wish to point out that the polymer microstructure postulated (in highly idealized form) by the B-PD model discussed briefly above also offers a possible explanation of the anomalous diffusion effect. In particular, the ballistic regime, which involves erratic collisions with ("rattling" against) the walls of the confining bundle of chains, should be commensurate with the *lateral* dimensions of the bundle, while anomalous diffusion would consist primarily of translation *along* the bundle, merging gradually into the normal diffusion regime when hops across the chains become sufficiently numerous. From this view, the extent of the observed anomalous diffusion regime is expected to depend on the degree to which the salient structural features of the B-PD model are realized in an actual amorphous polymer. The principal questions that arise in this respect are (i) whether there is significant local polymer chain orientation persisting over significant distances along the diffusion path and (ii) if so, whether the orientation of the observed displacement of the penetrant molecule over these distances tends to correlate with the said chain orientation.

It is noteworthy that evidence of a significant tendency toward local chain parallelism has already been adduced for short-chain polymethylene (decane and eicosane) model media studied by MD at a density typical of amorphous polyethylene.[17] Accordingly, it seemed to us worthwhile to compute and analyze MD trajectories for a typical gaseous penetrant in a model medium of this type, in order to seek answers to the above questions.

2. Model and Methods

MD Simulations Undertaken. Microcanonical (NVE) MD runs have been performed on a model system that resembles very closely the system of simulated amorphous short-chain polyethylene (density 0.86 g cm^{-3})−O_2 studied by Takeuchi and Okazaki.[18] The cubic MD box, subject to three-dimensional periodic boundary conditions, contained 30 united atom eicosane (C_{20}) chains with methylene and methyl groups treated as identical single particles (in the form of interpenetrating spheres, labeled B) and 20 spherical penetrant particles (simulating O_2 and designated A). The side length of the MD box was 2.55 nm, yielding a density of 0.84 g cm^{-3} based on the polymeric medium alone (0.91 g cm^{-3} based on the polymer plus oxygen), *i.e.*, slightly less than in ref 18.

Nonbonded A−A, B−B, and A−B interactions were represented by truncated 6−12 Lennard-Jones (LJ) potentials with characteristic energy and distance parameters ϵ and σ. Following refs 17 and 18, the values $\epsilon_B = 500$ J mol^{-1}, $\sigma_B = 0.38$

nm; $\epsilon_A = 940$ J mol^{-1}, $\sigma_A = 0.343$ nm; and $\epsilon_{AB} = (\epsilon_A\epsilon_B)^{1/2}$, $\sigma_{AB} = 1/2(\sigma_A + \sigma_B)$ were adopted. The B−B LJ potential acted between pairs of particles located on different chains and between fourth or more distant neighbors in the same chain. The cutoff distance was taken as $r_c = 2.1\sigma_B$ for all LJ interactions, as in ref 18. Intrachain bond stretching, bond angle bending, and internal rotation potentials identical to those of refs 17 and 18 were used. As already indicated, our intention was not to achieve an accurate potential parametrization for oxygen in polyethylene (or eicosane) but rather to keep within the context of the extensive body of existing mechanistic MD work based on this type of model medium.

The equations of motion were integrated using the velocity form of the Verlet algorithm[19] with a time step of 6.03 fs. Initial configurations were generated from an equilibrated LJ liquid of monomeric B particles, using 30 particles chosen at random (but within a specified minimum distance from one another) to serve as chain ends. Taking each chain end in turn, its nearest neighbor was designated as the next segment of the chain, and the process was repeated until all 30 20-particle chains were designated in this way. The remaining 20 free particles were then turned into A particles. The LJ potentials with drastically weakened attractive terms, in conjunction with correspondingly weakened bond stretching, bending, and torsional potentials, were then introduced and gradually brought up to full strength, while the MD algorithm was in operation to ensure smooth, continuous relaxation of the system under the changing conditions. Excess kinetic energy was removed periodically, and the system was guided toward the desired thermodynamic state by calling into operation suitable temperature and volume adjustment routines.[20] The latter routines were then switched off, and the system was allowed to settle, under NVE conditions, to its final state before production of the data to be used was begun. Attainment of the final state was indicated by the absence of any detectable systematic drift in temperature and pressure over ∼1 ns. The temperature and pressure attained were 303.5 ± 0.2 K and 161.3 ± 0.7 MPa, respectively. Here and in the following, values following the ± sign represent standard deviations of the mean (*i.e.*, standard deviations divided by the square root of the number of data points), unless otherwise indicated in the text. About 10 ns of production running time was necessary to secure a $\langle \Delta r_A^2 \rangle$ *versus* t plot displaying good linearity over ∼7 ns, on the basis of which a reliable value of the diffusivity D could be confidently estimated (see Figure 4 below). The data analyses were performed on records of all particle positions and velocities typically written on tape at 0.603 ps intervals. Shorter recording intervals (down to 0.024 ps) were employed for some runs, designed to explore short-time penetrant motion. To obtain good statistics, trajectory lengths of the order of 1 or 10 ns were found to be necessary for Figures 8−11 and 5−7, 12, respectively.

Reduced Trajectories. The fast local motion of the penetrant complicates its trajectory and makes the essential features of the diffusion mechanism more difficult to discern. Attempts to identify jump events (by defining as such all displacements δr exceeding an arbitrarily chosen minimum value δr_0 in a specified short time δt_0) and correlate them with sudden chain conformational changes have not led to any positive results.[6] Takeuchi and Okazaki[16] also identified jump events in a similar manner (the exact condition, as stated in their paper, being $\delta r > \delta r_0 \cap \delta t < \delta t_0$) with the additional requirement that the chosen values of δr_0 and δt_0 should lead to a value of the mean square jump length $\langle \delta r^2 \rangle$ consistent with the observed D and mean residence time between jumpts $\langle t_R \rangle$, *i.e.*, consistent with the relation

$$\langle \delta r^2 \rangle = 6 \langle t_R \rangle D \tag{1}$$

On this basis, Takeuchi and Okazaki obtained a spectrum of residence times in cavities. On the other hand, Pant and Boyd[21] have applied a coarse-graining technique, whereby the actual trajectory is replaced by sequences of time-averaged penetrant positions, corresponding to various short averaging times.

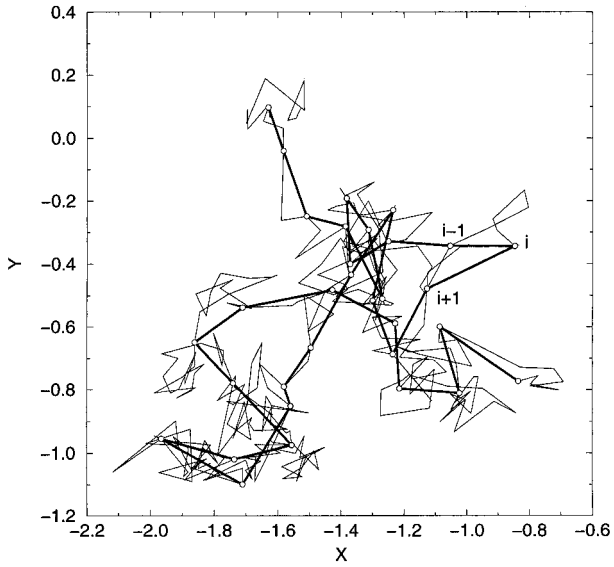

Figure 2. Example of the generation of a reduced trajectory of (nearly) constant step length (bold lines) from a recorded particle A trajectory (thin lines), as described in the text. The $x-y$ projections of both trajectories are shown. Distances are measured in half-edge length units from the center of the box.

A simpler, purely geometric approach is used in the present work. The recorded trajectory of each A particle is reduced to a number of successive positions i ($i = 0, 1, 2, ..., N$, where N is substantially smaller than the number of records) lying on the recorded trajectory at equal distances λ from one another (or nearly so, depending on the frequency of recording the original MD trajectory), or, equivalently, to a number of successive steps i ($i = 1, 2, ..., N$) of length λ (where step i joins positions $i - 1$ and i). Each position i is characterized by spatial ($\mathbf{r}_i$) as well as time (t_i) coordinates. A schematic of the trajectory reduction procedure is shown in Figure 2. This procedure was carried out for a number of λ values.

Characterization of Local Chain Orientation. The analysis presented in section 3 relies upon a quantitative characterization of local chain orientation in the polymer. With each B particle we associate a pentameric (trimeric) *subchain*, *i.e.*, a sequence of five (three) connected B particles centered at the particle in question. In the special case that the reference particle is next to a chain end, a tetramer starting at that end is considered in place of the pentameric subchain. In the case in which the reference particle is a chain end, a trimer (dimer) starting at the particle is considered in place of the pentameric (trimeric) subchain. The orientation of each subchain is characterized by a unit vector **u**, directed along the straight line that connects the first and last particles of the subchain. The **u** vectors of subchains are employed to (a) characterize the degree and direction of local orientation around specific points in the model system and (b) assess intramolecular orientational correlations along chains.

Given a position **r** in the model system, we identify neighboring subchains that dictate the local orientation in the vicinity of **r** by the following procedure. First, the radius R_{max} of a sphere centered at **r** (which defines the neighborhood of **r**) is chosen. R_{max} is large enough to encompass the first coordination shell of B particles (*i.e.*, the maximum of the A−B or B−B particle pair distribution function) whenever an A or B particle is used as the reference position **r**. A value of $R_{max} = 0.5$ nm was used here. This choice leads to a mean number of 9 trimeric, or 6.3 pentameric, neighboring subchains. The search for neighboring subchains starts by locating the B particle that is closest to **r**. The pentameric or trimeric subchain associated with the located B particle (in the sense described in the previous paragraph) is identified. Excluding all particles on the already identified subchain, we search for the next closest B, and this procedure is repeated until no further B particles can be found in the neighborhood of **r**. We define the tensor **Q**(**r**) as

$$\mathbf{Q}(\mathbf{r}) = \langle \mathbf{uu} \rangle_{\mathbf{r}} \tag{2}$$

where **uu** is the dyadic formed from the unit vector **u**, with elements $u^\alpha u^\beta$ ($\alpha,\beta = 1, 2, 3$) in a matrix representation in terms of the Cartesian components of **u**. In eq 2, the angular brackets denote arithmetic averaging over all subchains in the neighborhood of **r**, identified through the procedure described above. **Q**(**r**) thus constitutes a quantitative measure of the local orientation of the polymer around position **r**. Interestingly, a traceless version of **Q**(**r**) has been used to characterize macromolecular orientation in a recent MD study by Baljon *et al.*[22]

Diagonalization of **Q**(**r**) gives three real, nonnegative eigenvalues $L_1(\mathbf{r})^2 \geq L_2(\mathbf{r})^2 \geq L_3(\mathbf{r})^2$ with corresponding eigenvectors $\mathbf{v}_1(\mathbf{r})$, $\mathbf{v}_2(\mathbf{r})$, $\mathbf{v}_3(\mathbf{r})$. $\mathbf{v}_1(\mathbf{r})$ is the direction of the longest principal axis of the orientation ellipsoid around point **r**. It is used in the following as a descriptor of the prevalent direction of local chain orientation at **r**. L_1, L_2, and L_3 can be thought of as the lengths of the principal axes of the orientation ellipsoid at **r**. They satisfy the condition

$$L_1^{\,2} + L_2^{\,2} + L_3^{\,2} = Tr(\mathbf{Q}) = 1 \tag{3}$$

To characterize the shape of the local orientation ellipsoid, we define[23] the asphericity b as

$$b = L_1^{\,2} - {}^1/_2(L_2^{\,2} + L_3^{\,2}) = {}^1/_2(3L_1^{\,2} - 1) \tag{4}$$

the acylindricity c as

$$c = L_2^{\,2} - L_3^{\,2} \tag{5}$$

and the relative shape anisotropy κ^2 as

$$\kappa^2 = b^2 + {}^3/_4c^2 = {}^1/_2[(L_1^{\,2} - L_2^{\,2})^2 + (L_2^{\,2} - L_3^{\,2})^2 + (L_3^{\,2} - L_1^{\,2})^2] \tag{6}$$

The measures b and κ^2 vary from a value of zero for a completely isotropic orientation of subchains to unity in the case of perfect alignment along the direction $\mathbf{v}_1$.

Some of the calculations reported in section 3 call for a measure of local orientation of polymer subchains in relation to the orientation of corresponding steps of the reduced MD trajectory. A simple measure of this kind may be obtained by defining the local orientation tensor $\mathbf{Q}_{si}$ related to step i as

$$\mathbf{Q}_{si} = {}^1/_2[\mathbf{Q}(\mathbf{r}_{i-1}) + \mathbf{Q}(\mathbf{r}_i)] \tag{7}$$

Clearly, this definition is meaningful when step i is short enough for the subchain orientation around points $\mathbf{r}_{i-1}$ and $\mathbf{r}_i$ to be correlated. By diagonalizing $\mathbf{Q}_{si}$, one defines the longest principal axis direction $\mathbf{v}_{s1i}$ characterizing the prevalent orientation of polymer chains around step i, as well as the principal axis lengths $L_{s1i} \geq L_{s2i} \geq L_{s3i}$, exactly as explained above.

To analyze intramolecular orientational correlations, we consider pairs of subchains belonging to the same chain. Successive subchains overlap partly, so that the center of each subchain does not belong to any other subchain. More specifically, a total of six pentameric subchains are defined along each eicosane molecule, consisting of sites 1−5, 4−8, ..., 16−20. A total of nine trimeric subchains are defined along each eicosane molecule, consisting of sites 1−3, 3−6, ..., 17−19.

3. Results and Discussion

Hopping Motion and Anomalous Diffusion. Representative examples of the variation of the displacement $\Delta r_A(t) = |\mathbf{r}_A(t) - \mathbf{r}_A(0)|$ of A particles observed in a portion of a MD run is shown in Figure 3. Considerable diversity is seen in the shape of $\Delta r_A(t)$ curves among different particles. Clearly, under the conditions studied here, the penetrant motion is more complicated than a mere succession of jumps.

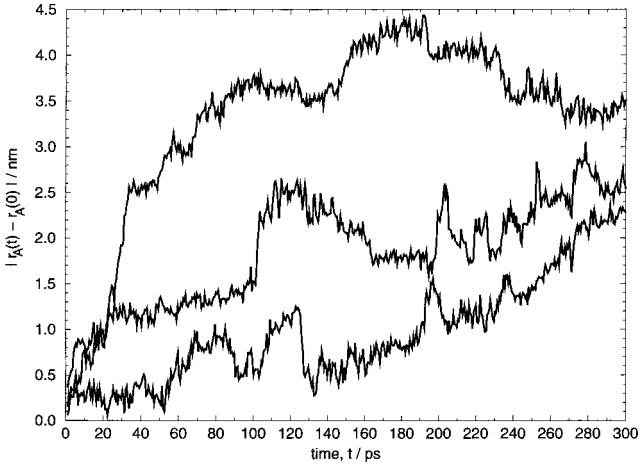

Figure 3. Magnitude of displacement as a function of time for three particle A trajectories.

The mean square displacement as a function of time, averaged over all time origins at 18 ps intervals and all 20 particle A trajectories, is shown in Figure 4, in both linear and log−log coordinates. The self-diffusivity value extracted from the slope of the linear part of this plot is $D_s = 2.7 \times 10^{-5}$ cm^2 s^{-1}, to be compared with 2.4×10^{-5} cm^2 s^{-1} given in ref 18 based on short (300 ps) MD runs and with 1.47×10^{-5} cm^2 s^{-1} given in ref 16 based on a MD run in a medium of this type but of "infinite" chain length (which is expected to reduce D). The log $\langle \Delta r_A^{\,2} \rangle$ *vs* log t plot brings out clearly the anomalous diffusion regime at short times. The Einstein regime sets in beyond $t \simeq 150$ ps or $\langle (\Delta r_A/\sigma_A)^2 \rangle \simeq 20$, corresponding to $\langle \Delta r_A^{\,2} \rangle^{1/2} \simeq 1.5$ nm.

Orientational Correlation between Steps of the Reduced Trajectory. Denoting the angle between steps i and j of the reduced trajectory of the penetrant by $\theta_{AA}(i,j)$,

$$\cos\theta_{AA}(i,j) = \frac{\mathbf{r}_i - \mathbf{r}_{i-1}}{|\mathbf{r}_i - \mathbf{r}_{i-1}|} \frac{\mathbf{r}_j - \mathbf{r}_{j-1}}{|\mathbf{r}_j - \mathbf{r}_{j-1}|} \tag{8}$$

we define the quantities

$$\langle \cos\theta_{AA}(n) \rangle = \langle \cos\theta_{AA}(i,i+n) \rangle \tag{9}$$

and

$$S_{AA}(n) = {}^1/_2(3\langle \cos^2\theta_{AA}(i,i+n) \rangle - 1) \tag{10}$$

which provide useful measures of the directional correlation between the ith and $(i + n)$th steps. The angular brackets on the right-hand sides of eq 9 and 10 denote averaging over all $i = 1, 2, ..., N - n$ along each reduced trajectory and over all 20 reduced trajectories. As illustrated in Figure 5, there is directional correlation between neighboring steps along a reduced trajectory, which is strongest between successive steps ($n = 1$) and tends to decay with increasing n more or less steeply for higher or lower λ, respectively. (In this and all subsequent figures, the height of error bars on each side of the relevant points equals the standard deviation of the mean of the displayed quantity over the duration of the MD run used to compute it.)

Interestingly, the directional correlation with $\lambda > 0.15$ nm seen in $\langle \cos\theta_{AA}(n) \rangle$ at low n values for reduced trajectories with $\lambda > 0.15$ nm is *negative*, indicating reversal of the direction of motion, consistent with a tendency of the penetrant molecule to move to and fro

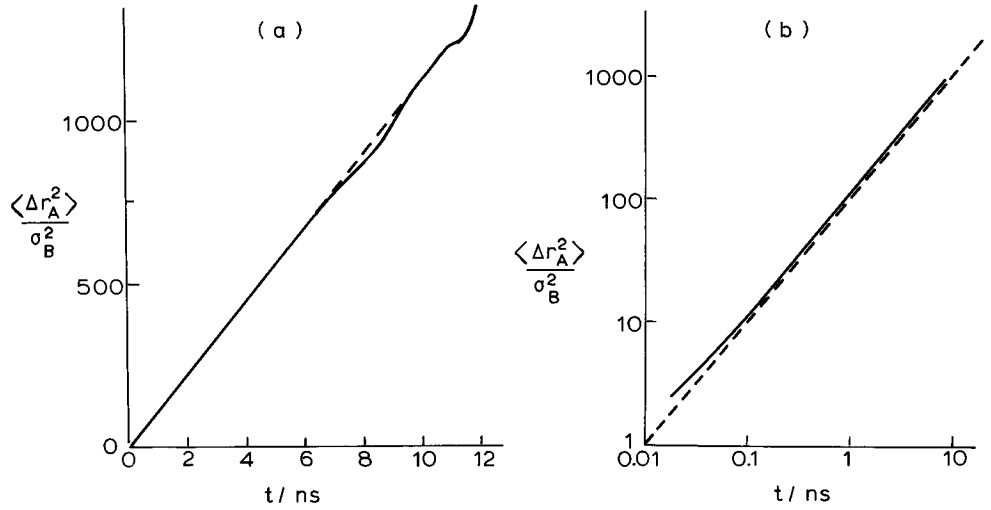

Figure 4. Mean square displacement *versus* time for A particles: (a) linear scales; (b) logarithmic scales, with slope of unity indicated by the broken line.

between opposite sides of a cavity in which it is temporarily trapped. From past geometric analyses,[9] cavities are expected to possess an elongated shape on the average. One can then distinguish two kinds of reciprocating motion of the penetrant, namely "shuttling", *i.e.*, long-range motion along the longest principal axis of the cavity, and "rattling", *i.e.*, short-range motion directed away from the said axis. Depending on the cavity shape and the step size λ, a reduced trajectory will tend to pick out more of the shuttling (larger λ) or rattling (smaller λ) motion.

The average quantities $\langle \cos \theta_{AA}(1) \rangle$ and $S_{AA}(1)$ between *successive* steps of the reduced trajectory are plotted as functions of the step size λ in Figure 6. In the region of negative $\langle \cos \theta_{AA}(1) \rangle$, $S_{AA}(1)$ and $|\langle \cos \theta_{AA}(1) \rangle|$ pass through a broad local maximum at $\lambda \simeq 0.3$; this suggests that the longest accessible dimension of the majority of cavities, along which shuttling occurs, is approximately equal to 0.3 nm (corresponding to ~0.6 nm wall to wall). The parallel decline of $S_{AA}(1)$ and $|\langle \cos \theta_{AA}(1) \rangle|$ as λ increases is presumably attributable to the fact that directionally uncorrelated intercavity jumps are sampled increasingly. Some evidence of shuttling motion is still discernible at quite high λ, however. This would be consistent with the presence of "easy pathways" along strings of cavities.

The decline of $S_{AA}(1)$ and $|\langle \cos \theta_{AA} \rangle|$ on the short λ side of the maximum, on the other hand, is consistent with progressive changeover from shuttling to more erratic rattling motion (*vide supra*). Below a certain λ, however, the behavior of $\langle \cos \theta_{AA}(1) \rangle$ ceases to mirror that of $S_{AA}(1)$. In particular, $S_{AA}(1)$ passes through a local minimum at $\lambda \simeq 0.15$ nm, while the trend in $\langle \cos \theta_{AA}(1) \rangle$ continues, leading to $\langle \cos \theta_{AA}(1) \rangle \simeq 0$ at the same point. Below $\lambda \simeq 0.15$ nm, $\langle \cos \theta_{AA}(1) \rangle$ becomes positive and exhibits an increasingly sharp tendency to rise, in parallel with $S_{AA}(1)$, as λ diminishes (ultimately attaining unity as $\lambda \rightarrow 0$). Obviously, in this region, the reduced trajectory increasingly picks up the ballistic motion of the penetrant molecule between collisions with the cavity walls.

To further elucidate the λ dependence of $\langle \cos \theta_{AA}(1) \rangle$ and $S_{AA}(1)$, full *probability distributions* of $\cos \theta_{AA}(1)$ values are presented in Figure 7 for four different step sizes λ of the reduced trajectory. In the same figure, the uniform distribution of $\cos \theta_{AA}(1)$ values characteristic of a random walk is displayed for comparison.

The fact that the distribution for large λ conforms most closely to the aforesaid uniform one is in keeping with the interpretation given above to the effect that the reduced trajectory here very largely tracks directionally uncorrelated intercavity jumps. Reduction of λ to a value approaching the maximum in $S_{AA}(1)$ and $|\langle \cos \theta_{AA}(1) \rangle|$ leads to substantial enrichment of the distribution in large negative $\cos \theta_{AA}(1)$ values (with corresponding deficiency in low negative and positive values), which is particularly marked for $\cos \theta_{AA}(1) \rightarrow -1$. This strong tendency for *sharp* reversal of the direction of motion confirms rather well the picture of shuttling along the long axis of elongated cavities of median length ~0.3 nm presented above.

The aforesaid enrichment in large negative $\cos \theta_{AA}$ values is reduced as λ decreases further and the distribution tends to become more uniform once again, consistent with the passage to more erratic rattling motion, as suggested above. Uniformity is not attained, however, because of the simultaneous tendency of the distribution to become increasingly enriched in larger positive $\cos \theta_{AA}(1)$ values. Thus, the distribution found at $\lambda = 0.15$ nm (corresponding to the minimum in $S_{AA}(1)$ and to $\langle \cos \theta_{AA}(1) \rangle \simeq 0$) is moderately enriched relative to the uniform one about equally in large positive and large negative $\cos \theta_{AA}(1)$ values; this is characteristic of reciprocating motion in small cavities or *across* median elongated cavities and of ballistic motion in large cavities or *along* median elongated cavities, respectively. Finally, as λ decreases further, the distribution becomes increasingly skewed, showing, as expected, increasing deficiency in rattling motion (negative $\cos \theta_{AA}(1)$ values) and enhancement of ballistic motion ($\cos \theta_{AA}(1) \rightarrow 1$ values).

The value of ~0.3 nm for prevalent accessible cavity size, arrived at by the above arguments, agrees well with the corresponding estimate obtained by Takeuchi and Okazaki through an entirely different analysis[15] (see preceding section). The shuttling motion in the confinement of cavities would make the reduced trajectory somewhat "denser" or more "nodular" than a true random walk. It is noteworthy that the occurrence of shuttling motion discovered here was anticipated by PD (*cf.* the statement: "a molecule would move backward and forward in its tube many times before jumping to an adjacent tube").[4]

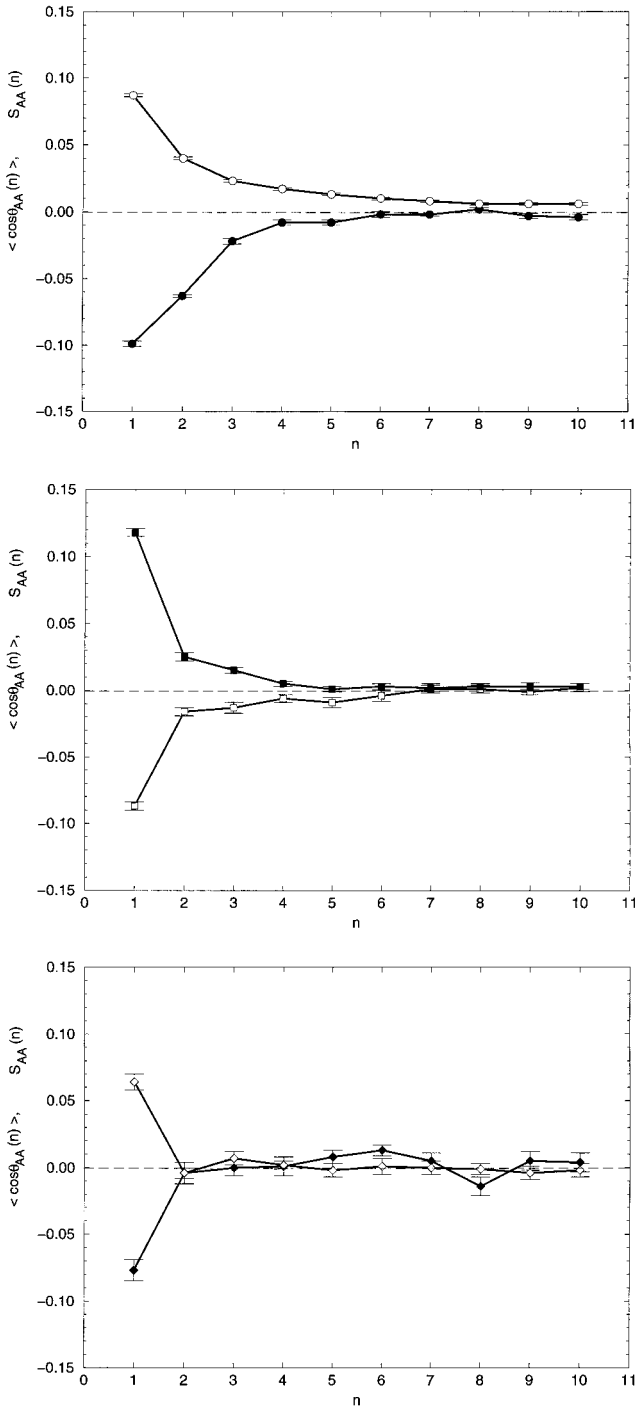

Figure 5. Quantities $\langle \cos \theta_{AA}(n) \rangle$ (lower plots) and $S_{AA}(n)$ (upper plots), indicative of orientational correlation between steps i and $i + n$ along the reduced trajectory of the penetrant, plotted as functions of n. Results are shown for three reduced trajectory step lengths: $\lambda = 0.198$ nm (circles); $\lambda = 0.351$ nm $\simeq \sigma_A$ (squares); and $\lambda = 0.694$ nm (diamonds).

Persistence of Polymer Orientation along the Diffusion Pathway. In keeping with the findings of Rigby and Roe,[17] a significant tendency toward local chain orientation was found, and its relaxation in space and time was studied in relation to the diffusion process.

Chain orientation in the vicinity of a diffusing A molecule changes with time because of the translational motion of A, which exposes it to different environments at different times, and also because the polymer matrix itself relaxes with time. It is instructive to compare the time scales of these two processes.

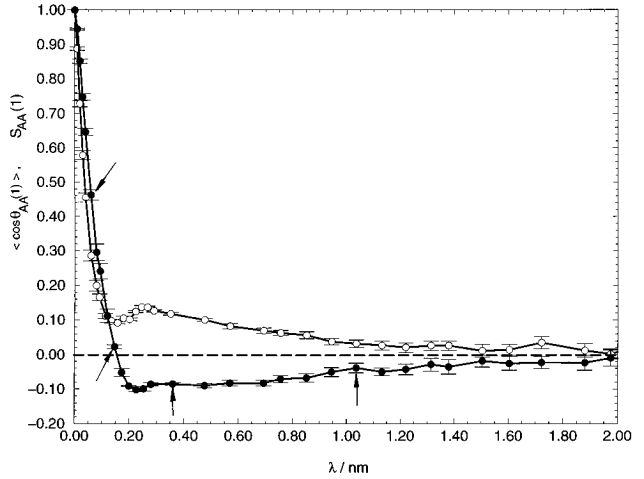

Figure 6. Measures of directional correlation between successive steps of the reduced trajectory, $S_{AA}(1)$ (○) and $\langle \cos \theta_{AA}(1) \rangle$ (●), plotted as functions of the step length λ. The points on the $\langle \cos \theta_{AA}(1) \rangle$ plot at which the probability distributions of $\cos \theta_{AA}(1)$ shown in Figure 7 were taken are shown by arrows.

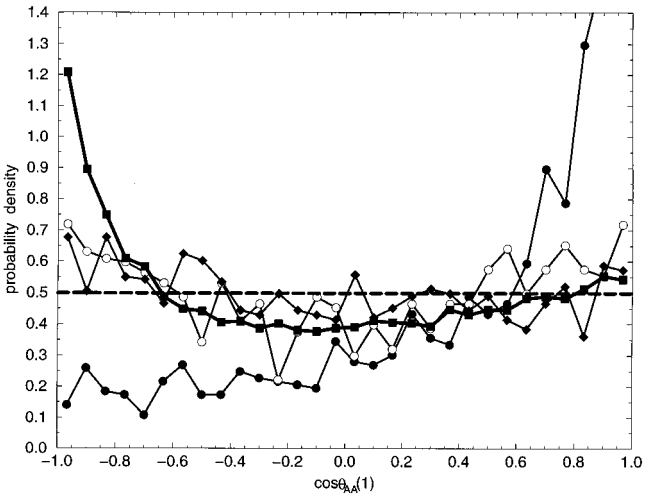

Figure 7. Normalized distribution of the cosine of the angle formed between successive steps of the reduced trajectory, $\cos \theta_{AA}(1)$, plotted for four different values of the step size: $\lambda = 0.06$ nm (●, thin line); $\lambda = 0.154$ nm (○, thin line); $\lambda = 0.351$ nm (■, bold line); and $\lambda = 1.038$ nm (◆, thin line). The bold broken line displays the uniform distribution that would correspond to a random path.

To characterize the rate of segmental reorientation in the polymer matrix, we choose N_P stationary sampling points $\mathbf{r}_k$, ($k = 1, 2, \ldots, N_P$) from a uniform distribution defined over the entire simulation box. From the unit eigenvectors $\mathbf{v}_1(\mathbf{r}_k,t_1)$ (determined as indicated in section 2), which describe the prevalent direction of orientation around sampling point $\mathbf{r}_k$ at time t_1, the orientational relaxation function $S_P(t)$ for the polymer matrix is computed as

$$S_P(t) = {}^1/_2\left[3\left\langle \frac{1}{N_P}\sum_{k=1}^{N_P}[\mathbf{v}_1(\mathbf{r}_k,t_1)\cdot\mathbf{v}_1(\mathbf{r}_k,t_1+t)]^2\right\rangle - 1\right] \quad (11)$$

where the angular brackets denote averaging over all available time origins t_1 in the stored dynamical trajectory.[19] $S_P(t)$ is a quantitative measure of the rate at which the memory of local orientation in the polymer matrix is lost as a result of thermal motion. $S_P(t)$, as computed from $N_P = 20$ sampling points, is shown in

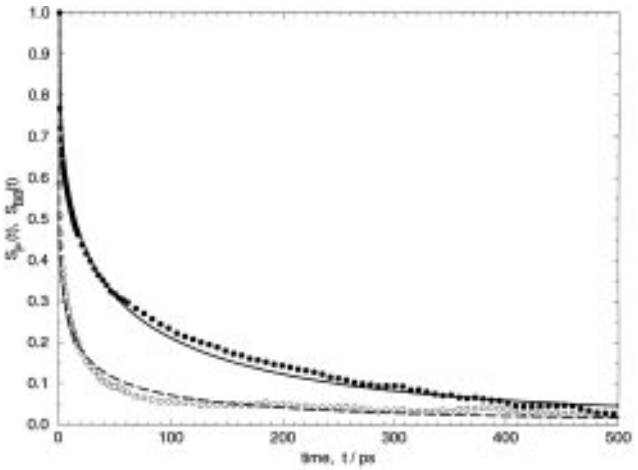

Figure 8. Relaxation functions of the unit vector describing the principal direction of segmental orientation at fixed, randomly selected points within the polymer matrix ($S_P(t)$, ●) and along the trajectory followed by the penetrant ($S_{BB}(t)$, ○). The principal direction of orientation was obtained from trimeric subchains. Stretched exponential fits to the two relaxation functions are shown as a solid ($S_P(t)$) and a broken line ($S_{BB}(t)$). See text for details.

Figure 8(filled symbols). The solid line represents a fit of the simulation data for $S_P(t)$ by a Kohlrausch−Williams−Watts (KWW) stretched exponential function

$$c_{KWW}(t) = \exp[-(t/\tau)^{\beta}] \qquad (12)$$

The KWW fit is not perfect; the initial part of $S_P(t)$ drops quasiexponentially, as has been pointed out in earlier relaxation studies.[24] Here we perform a KWW fit on the entire set of data, starting at $t = 0$, to facilitate comparison with previous MD simulation work. The best-fit parameters for $S_P(t)$ are $\tau = 35.5$ ps and $\beta = 0.430$. The stretching exponent is close to the value 0.50 used by Roe in melt simulations of polyethylene,[25] as well as to experimental values. The characteristic time τ lies between the values of 95.2 and 11.3 ps obtained by Takeuchi and Roe[26] from KWW fits of the autocorrelation functions of trimer subchain and out-of-plane vectors, respectively, in an infinite-chain polyethylene under similar conditions.

To quantify the rate of change in the local polymer orientation actually "seen" by the diffusing penetrant molecules, we follow the recorded trajectory $\mathbf{r}_A(t)$ of each penetrant molecule and examine the correlation between the prevalent local subchain orientation at position $\mathbf{r}_A(t_1)$ with that at a subsequent position $\mathbf{r}_A(t_1 + t)$. We define the orientational relaxation function $S_{BB}(t)$ around the penetrant trajectory as

$$S_{BB}(t) = {}^1/_2[3\langle[\mathbf{v}_1(\mathbf{r}_A(t_1))\cdot\mathbf{v}_1(\mathbf{r}_A(t_1 + t))]^2\rangle - 1] \qquad (13)$$

where the angular brackets denote averaging over all available time origins t_1 and over all A molecules. $S_{BB}(t)$ is displayed in Figure 8 (open symbols). It is described reasonably satisfactorily by a KWW stretched exponential function (eq 12) with $\tau = 2.88$ ps and $\beta = 0.275$ (broken line in Figure 8). The small value of the stretching exponent points to the multiplicity of time scales characterizing the motion of the diffusing penetrant.

Comparing $S_P(t)$ and $S_{BB}(t)$, we observe immediately that the loss of orientational correlation seen by the moving penetrant stems mainly from the displacement of the penetrant itself. Even in the short-chain melt studied here, the relaxation of the polymer matrix is at least an order of magnitude slower than translational motion of the penetrant.

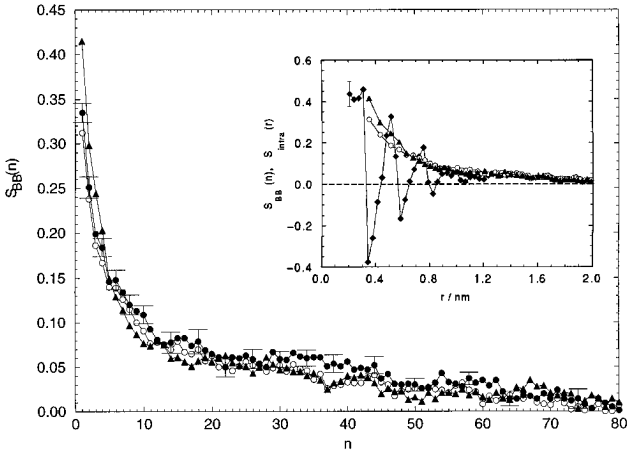

Figure 9. Persistence of polymer orientation along the reduced trajectory of a penetrant molecule. The orientational correlation parameter $S_{BB}(n)$ is shown as a function of the number of steps n, as calculated from pentameric (●) or trimeric (○) subchains neighboring the nodes of the reduced trajectory. Also shown is $S_{BB}(n)$ from pentameric subchains along a random path generated in the polymer as described in the text (▲). The step length for both actual and random trajectories is $\lambda = 0.351$ nm $\simeq \sigma_A$. Inset: Orientational correlation along the polymer chains in comparison with the persistence of orientation seen by the diffusing penetrant. The orientational correlation parameter $S_{BB}(n)$ along the reduced trajectory and along the random path is shown as a function of the spatial distance r between nodes. The plotting symbols and λ values are as stated above. Also shown is the intramolecular orientational correlation parameter $S_{intra}(r)$ between trimeric subchains belonging to the same chain (◆). Along the intramolecular curve, error bars for all but the first point are comparable in size to the plotting symbols.

An alternative way of displaying the degree of persistence of chain orientation along the path of the penetrant is adopted in Figure 9. Here, the penetrant positions $\mathbf{r}_A(t)$ considered in eq 13 are replaced by the nodes $\mathbf{r}_i(t_i)$ along a reduced trajectory of given step length λ, and S_{BB} is accumulated as a function of the number of steps n between the nodes:

$$S_{BB}(n) = {}^1/_2[3\langle[\mathbf{v}_1(\mathbf{r}_i)\cdot\mathbf{v}_1(\mathbf{r}_{i+n})]^2\rangle - 1] \qquad (14)$$

The brackets in eq 14 denote averaging over all nodes i on all reduced trajectories of given λ for which both $\mathbf{r}_i$ and $\mathbf{r}_{i+n}$ exist. The unit vector $\mathbf{v}_1(\mathbf{r}_i)$ describing the prevalent orientation of the polymer around each node $\mathbf{r}_i(t_i)$ is obtained as explained in section 2. On the average, 6.3 pentameric subchains are found neighboring each node of the reduced trajectory. Of the 15−20 pairs formed by these subchains, 1.5 on the average belong to the same chain. Thus, $S_{BB}(n)$ is shaped by both inter- and intramolecular orientational tendencies in the polymer.

$S_{BB}(n)$, as calculated from reduced penetrant trajectories of step length $\lambda = 0.351$ nm $\simeq \sigma_A$, is displayed in Figure 9. Results derived from pentameric and trimeric subchains are identical within the error of the simulation. The degree of persistence of local chain orientation of chains drops to values around $S_{BB} = 0.10$ within 10 steps of the reduced trajectory and then decays to zero over the next 75 steps or so.

To assess whether this persistence of orientation is particular to the paths followed by the diffusing penetrant or a more general characteristic of the polymer

matrix, we generated "random paths" of ghost A particles, as counterparts of actual reduced MD trajectories of given step length λ. Each successive position $\mathbf{r}_i$ constituting the random path is chosen randomly on the circumference of a sphere of radius λ centered at $\mathbf{r}_{i-1}$, assuming zero A−A and A−B interactions but assigning the same time coordinate as for the ith position of the corresponding real trajectory. Thus, the temporal evolution of the polymer is built into the generation of random paths. It is noteworthy that $S_{BB}(n)$ along a random path, displayed in Figure 9 (▲), does not differ materially from $S_{BB}(n)$ along the corresponding actual reduced trajectory (except that it tends to be distinctly higher at small n values for reasons to be explained below). Thus, the persistence of orientation shown by $S_{BB}(n)$ seems to be an intrinsic characteristic of the microstructure of the polymer in its entirely, rather than of the specific paths followed by the pentrant molecule. A replot of $S_{BB}(n)$ as a function of the spatial displacement of the penetrant molecule Δr_A (see inset to Figure 9) shows that memory of the local chain orientation at the origin of the displacement is completely effaced only beyond $\Delta r_A \simeq 2$ nm and is, therefore, sufficiently long-range to encompass the region of anomalous diffusion. This is, to our knowledge, the first concrete envidence of a *specific* microstructural feature that might plausibly be supposed to be implicated in the anomalous diffusion phenomenon.

To what extent is the persistence of orientation seen in $S_{BB}(n)$ a result of intramolecular correlations along individual macromolecules (chain stiffness)? Also plotted in the inset to Figure 9 is the intramolecular orientation correlation function $S_{intra}(r)$ between trimeric subchains on the same chain. The cosine of the angle between the end-to-end vectors of each pair of subchains belonging to the same molecule was obtained and used to evaluate the order parameter S_{intra} (compare eq 10). S_{intra} was binned according to the distance r between subchain centers and averaged over all chains and all configurations to obtain $S_{intra}(r)$. The result exhibits pronounced maxima and minima, due to the conformational preferences of single chains.[27] S_{intra} decays to zero over a distance comparable to the decay length of $S_{BB}(n)$. Thus, the persistence of orientation exhibited by S_{BB} seems to originate, in part, from orientational correlations along individual chains in the model system.

Degree of Local Polymer Orientation. The discussion above concerned the prevalent *direction*, but not the *degree*, of local orientation in the polymer. The latter follows from the measures b and κ^2, characteristic of the shape of the local orientation ellipsoids, deduced from the relevant $\mathbf{Q}(\mathbf{r}_i)$ tensors as described in section 2. Results obtained for the nodes of actual reduced trajectories were compared with those for the corresponding random paths. In Table 1 are shown the average $\langle b \rangle$ and $\langle \kappa^2 \rangle$ values obtained, and good statistics is demonstrated by agreement of the results from different λ. There is a distinct difference, however, in the degree of anisotropy of the orientational environment between nodes of actual reduced trajectories and those of random trajectories. The former is characterized by mean asphericity 0.40 and mean relative shape anisotropy 0.21 (corresponding roughly to an ellipsoid with principal axes in the ratio $L_1:L_2:L_3 = 2.9:2.2:1.0$), as against a mean asphericity of 0.50 and a mean relative shape anisotropy of 0.31 (corresponding roughly to an ellipsoid with principal axes in the ratio $L_1:L_2:L_3 = 5.2:3.5:1.0$) for the latter. This difference is in line with expectation, since denser chain packing (which favors a higher degree of alignment of the polymer chains[17] because of the stronger attractive nonbonded interactions between them) is more likely in the absence of a penetrant molecule (random path nodes) than in its presence (actual trajectory nodes). Note that this difference also explains why S_{BB} for the random path in Figure 9 is distinctly higher at small n than that for the real reduced trajectory. We emphasize that this higher degree of orientation seen along the random path is simply due to the absence of A molecules, which allows polymer chains to come closer together.

Table 1. Characteristics of the Local Orientation around the Reduced Trajectory of a Penetrant and around a Random Path Generated in the Polymer[a]

		λ, nm				
		0.198	0.351	0.694	1.379	2.056
actual path	$\langle b \rangle$	0.393	0.399	0.394	0.407	0.399
	$\langle \kappa^2 \rangle$	0.207	0.212	0.212	0.218	0.211
random path	$\langle b \rangle$	0.505	0.496	0.508	0.492	0.511
	$\langle \kappa^2 \rangle$	0.328	0.318	0.334	0.305	0.330

[a] $\langle b \rangle$ is the mean asphericity and $\langle \kappa^2 \rangle$ the mean relative shape anisotropy of the local orientation ellipsoids. Results, as obtained from pentameric subchains, are shown for different values of the step length λ.

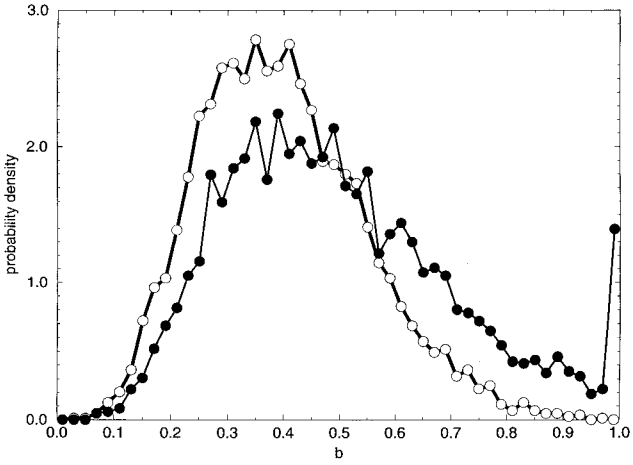

Figure 10. Probability distribution of asphericities b of the local chain orientation around an actual reduced trajectory of the penetrant (○, bold line) and around a random trajectory (●, thin line), with step length $\lambda = 0.351$ nm in each case. Orientation tensors were computed from pentameric subchains.

The full distributions of b and κ^2 values encountered around actual penetrant and random trajectories are shown in Figures 10 and 11, respectively. (Values reported in Table 1 are averages over these distributions.) All distributions are broad, reflecting the multiplicity of local orientational environments within the melt. The distributions around the random trajectories are broader, with a larger contribution from high values than those around the actual trajectories. This again shows the lower degree of orientational anisotropy prevailing around nodes of actual penetrant trajectories. Remarkably, the random path probability densities assume substantial nonzero values at $b \rightarrow 1$ and $\kappa^2 \rightarrow 1$, indicating the presence of microregions in the melt in which neighboring chain segments approach perfect alignment. Such regions are not encountered in real trajectories, because they are of necessity dense and hence cannot form in the presence of A molecules.

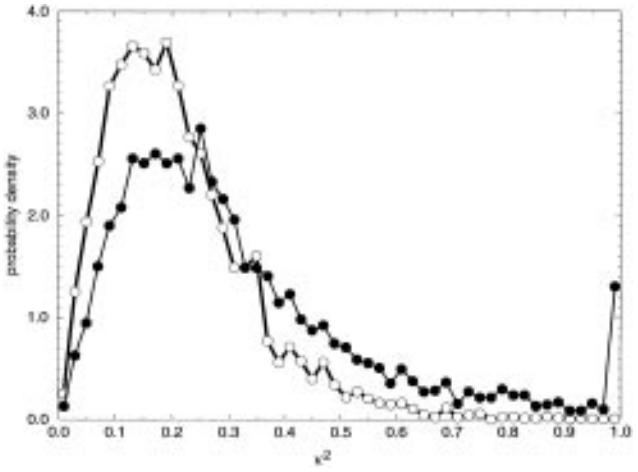

Figure 11. Probability distribution of relative shape anisotropies κ^2 of the local chain orientation around an actual reduced trajectory of the penetrant (○, bold line) and around a random reduced trajectory (●, thin line), with step length $\lambda = 0.351$ nm in each case. Orientation tensors were computed from pentameric subchains.

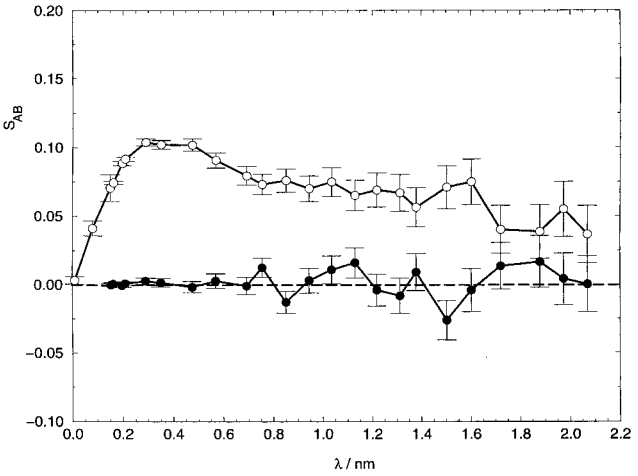

Figure 12. Orientational correlation parameter S_{AB} between steps of the reduced trajectory of a penetrant and the local orientation of the surrounding polymer, plotted as a function of the step length of the reduced trajectory λ (○). Also shown is the plot for the corresponding random path (●).

Orientational Correlation between Penetrant Motion and Surrounding Chains. Is there any coupling between the overall direction of displacement of a penetrant molecule and the prevalent orientation of the surrounding polymer chains? To address this question, we considered reduced trajectories with a variety of step lengths. Through diagonalization of the orientation tensors $\mathbf{Q}_{si}$, defined in eq 7, we determined the unit vectors $\mathbf{v}_{s1i}$ characterizing the orientation of the polymer around each step i of each reduced trajectory. For each such step, we formed the quantity

$$\cos\theta_{AB}(i) = \frac{\mathbf{r}_i - \mathbf{r}_{i-1}}{|\mathbf{r}_i - \mathbf{r}_{i-1}|}\,\mathbf{v}_{s1i} \qquad (15)$$

and computed the direction correlation parameter

$$S_{AB} = {}^1/_2(3\langle\cos^2\theta_{AB}(i)\rangle - 1) \qquad (16)$$

where the angular brackets signify averaging over all steps and all reduced trajectories of a given step length λ. S_{AB} is displayed as a function of λ in Figure 12.

Figure 12 establishes unequivocally that there is some directional correlation between the steps of the reduced trajectory of a penetrant and the orientation of the surrounding polymer. S_{AB} displays a broad maximum around $\lambda = \sigma_A$, which matches remarkably well that in $S_{AA}(1)$, discussed earlier in conjunction with Figure 6. Thus, we now have clear evidence that the shuttling motion of the penetrant tends to occur along the direction of local chain orientation. This is consistent (i) with the expectation that the longest dimension of anisotropic cavities (and, to a lesser extent, of clusters of cavities) will tend to be parallel to the surrounding chains and (ii) with the predictions of the B-PD model. The decay of S_{AB} for smaller and for larger λ is attributable to the same causes as that of $S_{AA}(1)$: for shorter λ, the steps of the reduced trajectory increasingly pick up the short-range erratic rattling motion within cavities, while for longer λ, they increasingly include intercavity jumps. The length scale over which S_{AB} remains nonzero is ~1.5 nm and is, therefore, also entirely comparable with the maximum extent of anomalous diffusion effects (compare Figure 4 and discussion above).

As a control, S_{AB} has also been determined along the corresponding random trajectories generated in the polymer and is also shown in Figure 12 as a function of λ. Clearly, the directional correlation between path step and surrounding chains is zero in the case of random paths for all length scales.

Figure 12 furnishes crucial evidence in favor of the argument linking the persistence of chain orientation shown in Figure 9 with the anomalous diffusion regime, by demonstrating a direct effect of the said structural feature on penetrant motion. Note, however, that the structural feature in question does not restrict penetrant motion, as suggested in ref 6 (except in an orientational sense), but rather tends to provide an "easy pathway" for the penetrant molecule, as suggested by the B-PD model. A realistic picture for the said easy pathways is that of elongated strings of cavities, which extend considerably farther than indicated by the median cavity size of 0.3 nm[15] but do not constitute a connected network.

4. Conclusions

We have undertaken a geometric analysis of long (up to 10 ns) MD trajectories of spherical oxygen-like (A) molecules dissolved in a melt of short polymethylene-like (B_{20}) chains at a density near that of amorphous polyethylene to study mechanistic aspects of penetrant motion. The potential representation was chosen with a view toward facilitating comparison with earlier mechanistic simulation work.

Two new tools have been introduced to enable a meaningful geometric analysis of motion in real space. The first is the concept of a "reduced trajectory". This is defined as a set of positions $\mathbf{r}_i$ (associated with the corresponding times t_i) along the actual path of an A molecule, successive positions lying at a fixed distance λ from each other. By using reduced trajectories with appropriate λ in place of the full recorded trajectories, one can focus on the transport model prevailing at specific length scales. The second tool is a technique for quantifying the local orientation around specific nodes or steps of the reduced trajectory (or around any chosen point or short line in the polymer matrix). This technique is based on accumulating a local orientation tensor $\mathbf{Q}(\mathbf{r})$ or $\mathbf{Q}_{si}$ from the end-to-end vectors of short

(trimeric or pentameric) subchains in the vicinity of the considered node or step (see eqs 2 and 7). The eigenvector $\mathbf{v}_1$ or $\mathbf{v}_{s1i}$, corresponding to the largest eigenvalue of **Q**, characterizes the prevalent direction of local orientation, while the eigenvalues are used to form shape measures characteristic of the type and degree of local orientational anisotropy (see eqs 4 and 6). In addition to the penetrant reduced trajectories, random trajectories of ghost A molecules, of step length λ, have been generated through the temporally evolving polymer configuration, to assess what (if anything) is special about the actual path traversed by the penetrant. These analytical tools are likely to prove to be of more general utility for the study of the microstructure of amorphous polymeric media and of micromolecular transport therein.

Three types of directional correlation parameters have been considered in our analysis: S_{BB} (see eqs 13 and 14) measures the persistence of local polymer orientation along a specified path; S_{AB}(eq 16) measures the directional correlation between penetrant motion and local chain orientation; and $\langle \cos \theta_{AA} \rangle$ and S_{AA} (eqs 9 and 10) measure the directional correlation between different steps along a reduced trajectory.

As in earlier simulation work, an anomalous diffusion regime ($\langle \Delta r_A^2 \rangle \propto t^n$, with $n < 1$) was detected, which extends up to $t \simeq 150$ ps or $\langle \Delta r_A^2 \rangle^{1/2} \simeq 1.5$ nm (Figure 3). The results reported here show that considerable insight into the causes of this anomalous kinetic regime can be gained by judicious utilization of the aforementioned directional correlation parameters.

Even for the amorphous, short-chain model polymeric medium considered here, the decay of local chain orientation, induced by thermal motion, is found to be slow by comparison with the rate of migration of penetrant molecules ($S_P(t)$ *vs* $S_{BB}(t)$ in Figure 8). In addition to (but partly as a result of) this, we find detectable persistence of local chain orientation, as measured by $S_{BB}(n)$ (see Figure 9), along a typical penetrant molecule trajectory over distances as long as 2 nm, which is shown to be an intrinsic structural characteristic of the polymer matrix.

Polymer microstructure has previously been suggested as the cause of anomalous diffusion.[6,15] Here, we have identified a specific microstructural feature which is commensurate with the anomalous diffusion regime. This significant result is taken one crucial step further by the demonstration, through S_{AB} (see Figure 12), of a definite tendency of penetrant motion to follow local chain orientation, as required for a full answer to questions (i) and (ii) raised in the Introduction. The aforementioned tendency is, furthermore, strongly correlated with the occurrence of shuttling motion revealed by $S_{AA}(1)$ and $\langle \cos \theta_{AA}(1) \rangle$ (see Figure 6), as expected on the basis of the B-PD model picture. Both S_{AB} and S_{AA}-(1) (*cf.* Figures 6 and 12) attain maximum values on a length scale of $\lambda \simeq 0.3$ nm, consistent with the presence of elongated cavities of this accessible median length (in agreement with conclusions drawn from other types of analysis[9,15]), and still discernibly exceed zero at $\lambda \simeq 1.5$ nm, consistent with the presence of strings of cavities providing relatively facile penetrant pathways on this length scale. On the low λ side, $\cos \theta_{AA}$ spectra offer a particularly clear picture of longer-range axial shuttling motion changing over to more disordered, predominantly lateral, short-range rattling motion and then to ballistic motion as λ decreases and ultimately approaches zero.

We conclude that (a) some salient microstructural features of the B-PD model can definitely be discerned, albeit in very attenuated form, in the much more realistic model amorphous polymeric medium considered here and (b) the occurrence of the anomalous diffusion regime is most likely intimately related to these features.

Acknowledgment. The authors express their appreciation to Drs. Hisao Takeuchi and Michael Greenfield and to Professor A. Panagiotopoulos for stimulating discussions. Dr. Takeuchi is thanked for making his manuscript[15] available prior to publication.

References and Notes

(1) Glasstone, S.; Laidler, K. J.; Eyring, H. *Theory of Rate Processes*; McGraw-Hill: New York, 1941.
(2) Crank, J.; Park, G. S. *Diffusion in Polymers*; Academic Press: New York, 1968.
(3) Brandt, W. W. *J. Phys. Chem.* **1959**, *63*, 1080.
(4) Pace, R. J.; Datyner, A. *J. Polym. Sci., Polym. Phys. Ed.* **1979**, *17*, 437, 453, 465.
(5) Petropoulos, J. H. In *Polymeric Gas Separation Membranes*; Paul, D. R., Yampolski, Yu. P., Eds.; CRC Press: Boca Raton, FL, 1994; Chapter 2.
(6) Gusev, A. A.; Müller-Plathe, F.; van Gunsteren, W. R.; Suter, U. W. *Adv. Polym. Sci.* **1994**, *116*, 207.
(7) Theodorou, D. N. In *Diffusion in Polymers*; Neogi, P., Ed.; Marcel Dekker: New York, 1996.
(8) Arizzi, S.; Mott, P.; Suter, U. *J. Polym. Sci., Polym. Phys. Ed.* **1992**, *30*, 415.
(9) Greenfield, M. L.; Theodorou, D. N. *Macromolecules* **1993**, *26*, 5461.
(10) Gusev, A. A.; Arizzi, S.; Suter, U. W.; Moll, D. J. *J. Chem. Phys.* **1993**, *99*, 2221.
(11) Greenfield, M. L.; Theodorou, D. N. *Polymeric Materials: Science and Engineering*; American Chemical Society: Washington, DC, **1994**; Vol. 71, p 407.
(12) Müller-Plathe, F.; Rogers, S. C.; van Gunsteren, W. F. *Chem. Phys. Lett.* **1992**, *199*, 237.
(13) Kremer, K.; Grest, G. S.; Robbins, M. O. *J. Phys. A: Math. Gen.* **1987**, *20*, L181.
(14) Hwang, Y. H.; Wu, X.-l. *Phys. Rev. Lett.* **1995**, *74*, 2284.
(15) Takeuchi, H.; Okazaki, K. *Mol. Simul.*, in press.
(16) Takeuchi, H.; Okazaki, K. *Kobunshi Ronbunshu* **1994**, *51*, 387.
(17) Rigby, D.; Roe, R.-J. *J. Chem. Phys.* **1988**, *89*, 5280.
(18) Takeuchi, H.; Okazaki, K. *J. Chem. Phys.* **1990**, *92*, 5643.
(19) Allen, M. P.; Tildesley, D. J. *Computer Simulation of Liquids*; Clarendon: Oxford, UK, 1987.
(20) Fincham, D.; Heyes, D. M. *Adv. Chem. Phys.* **1985**, *63*, 493.
(21) Pant, P. V. K.; Boyd, R. H. *Macromolecules* **1993**, *26*, 679.
(22) Baljon, A. R. C.; Grest, G. S.; Witten, T. A. *Macromolecules* **1995**, *28*, 1835.
(23) Theodorou, D. N.; Suter, U. W. *Macromolecules* **1985**, *18*, 1206.
(24) Ngai, K. L.; Rendell, R. W.; Rajakopal, A. K.; Teitler, S. *Ann. N. Y. Acad. Sci.* **1986**, *484*, 150.
(25) Roe, R.-J. *Adv. Polym. Sci.* **1994**, *116*, 112.
(26) Takeuchi, T.; Roe, R.-J. *J. Chem. Phys.* **1991**, *94*, 7446.
(27) Theodorou, D. N.; Suter, U. W. *Macromolecules* **1985**, *18*, 1467.

MA951474Z